A Vector-Based Constrained Obstacle Avoidance Scheme for Wheeled Mobile Redundant Robot Manipulator

Zhijun Zhang, *Senior Member, IEEE*, Song Yang, Siyuan Chen, Yamei Luo, Hui Yang, and Yu Liu, *Member, IEEE*

***Abstract*—Obstacle avoidance is an important issue when a wheeled mobile redundant robot manipulator (WMRRM) completes given tasks in complex environment. In this article, a novel vector-based constrained obstacle avoidance (VOA) scheme is designed and analyzed for motion planning of the WMRRM. Specifically, the VOA scheme is first described as a quadratic programming (QP) problem subject to an equality constraint, an inequality constraint, and a bound constraint. Compared with the traditional obstacle avoidance scheme, the proposed VOA scheme can not only achieve subtasks, such as obstacle avoidance and physical limit avoidance when the robot completes the main end-effector task, but also greatly expands the range of feasible spaces. In addition, the VOA scheme is transformed into piecewise linear projection equations (PLPEs) and solved by a linear-variational-inequality-based primal–dual neural network (LVI-PDNN), which can efficiently obtain the optimal solutions to the VOA scheme. Computer simulations demonstrate the reliability, accuracy, and effectiveness of the proposed VOA scheme.**

***Index Terms*—Linear-variational-inequality-based primal–dual neural network (LVI-PDNN), obstacle avoidance, quadratic programming (QP), wheeled mobile redundant robot manipulator (WMRRM).**

Manuscript received August 22, 2019; revised January 19, 2020; accepted February 20, 2020. Date of publication March 9, 2020; date of current version September 9, 2021. This work was supported in part by the National Natural Science Foundation under Grant 61976096, Grant 61603142, Grant 61633010, Grant 61733005, and Grant 61673172; in part by the Guangdong Foundation for Distinguished Young Scholars under Grant 2017A030306009; in part by the Guangdong Special Support Program under Grant 2017TQ04X475; in part by the Science and Technology Program of Guangzhou under Grant 201707010225; in part by the Fundamental Research Funds for Central Universities under Grant x2zdD2182410; in part by the Scientific Research Starting Foundation of South China University of Technology; in part by the National Key Research and Development Program of China under Grant 2017YFB1002505; in part by the National Key Basic Research Program of China (973 Program) under Grant 2015CB351703; in part by the Guangdong Key Research and Development Program under Grant 2018B030339001; and in part by the Guangdong Natural Science Foundation Research Team Program under Grant 1414060000024. *(Corresponding authors: Zhijun Zhang; Yu Liu.)*

Zhijun Zhang, Song Yang, Siyuan Chen, Yamei Luo, and Yu Liu are with the School of Automation Science and Engineering, South China University of Technology, Guangzhou 510640, China (e-mail: drzhangzhijun@gmail.com; auyangsong@mail.scut.edu.cn; c.sy05@mail.scut.edu.cn; phmeihua@126.com; auylau@scut.edu.cn).

Hui Yang is with the Key Laboratory of Advanced Control and Optimization of Jiangxi Province, School of Electrical and Automation Engineering, East China Jiaotong University, Nanchang 330013, China (e-mail: yhshuo@263.net).

Color versions of one or more figures in this article are available at https://doi.org/10.1109/TCDS.2020.2979340.

Digital Object Identifier 10.1109/TCDS.2020.2979340

I. Introduction

In recent years, robot manipulators have been widely applied to various fields, [1]–[11], such as automatic assembly lines in factories [4]–[6], intelligent catering services [9], precision medical operations [7], [8], and the disaster relief [10], [11]. The application scenarios mentioned above require the high flexibility of the robot manipulators. The redundant robot manipulator is a kind of flexible robot manipulator and it is preferred because it can accomplish some subtasks when the robot manipulator is finishing the main end-effector task. Especially, mobile redundant manipulators have many advantages than fixed redundant manipulators. For instance, mobile redundant manipulators have larger working spaces and higher flexibilities. Therefore, mobile redundant manipulators have been applied to many areas. One important application is the wheeled mobile redundant robot manipulator (WMRRM) for disabled patients.

Considering a disabled patient in a wheelchair, a redundant manipulator embedded on a wheelchair can help the patient to deal with some daily tasks. In Fig. 1, a WMRRM designed by our lab is shown. It includes a differential driven wheelchair, a 6 degrees-of-freedom manipulator, and a three-fingered dexterous hand. The disabled person can control the WMRRM to move to an expected place, grasp an object (such as a cup) to his/her desired place (such as his/her mouth).

In order to control the WMRRM, the inverse kinematic problem is an unavoidable problem. It is to obtain the angular value of each joint corresponding to the robot manipulator and the angular value of each driving wheel when the target trajectory of the end effector is given. However, obtaining the analytical solution to the inverse kinematic problem is hard because of the nonlinearity of the mapping function in the kinematic equation. In addition, there exist infinite solutions because WMRRM is a redundant robot system.

A common method for solving the inverse kinematic is to establish the kinematic equation at the velocity level. There were many schemes have been put forward to solve the inverse kinematic problem of the redundant robot manipulator in previous years [12], [13]. The pseudoinverse method is an effective traditional method to solve the inverse kinematic problem [14]–[16]. However, the inequality constraints cannot be considered by the pseudoinverse and it is hard to design secondary optimal criterion. In addition,

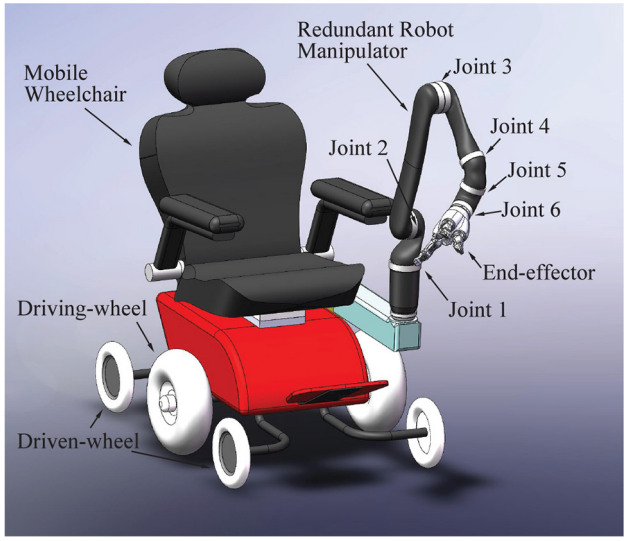

Fig. 1. Computer modeling graphic of the mobile wheelchair equipped with a redundant robot manipulator.

the computation of inverse/pseudoinverse of matrices is usually considered as a time-consuming work. The quadratic programming (QP)-based method has been widely applied to robot control in recent years [17]–[19], because the secondary subtasks are very easy to be designed as optimization criteria or equality/inequality constraints in a QP problem [20]–[22].

In practical applications, obstacles always exist, and thus obstacle avoidance should be considered in the motion planning scheme of the WMRRM. The traditional methods of obstacle avoidance for mobile robots are based on artificial potential field [23], [24]. In the virtual artificial potential field, the mobile robot can obtain a driving force consisting of the attraction of the target point and the repulsion of the obstacle [24]. However, it is not flexible to use the resultant force to achieve the obstacle avoidance of the WMRRM because the redundant manipulator equipped on the wheelchair has the characteristics of multiple joints and strong coupling [23]–[25]. As pointed out in [21], [22], and [26], obstacle avoidance was easily formulated as an inequality constraint and incorporated directly into the QP-based scheme. In [21], a method for obstacle avoidance based on maximizing the distance between links of the robot manipulator and obstacles was proposed. However, calculating the derivative of the distance function can bring the heavy computational burden and it is unfavorable for real-time applications of the robot control system. The obstacle avoidance was described as a dynamic equality constraint in [26]. However, the suitable magnitude of escape velocity of robot is hard to determine. The obstacle avoidance scheme in [22] limited the flexibility of the redundant robot because the arithmetical operation between the scalar signum function $\mathrm{sgn}(\cdot)$ and the Jacobian matrix made the scalar signum function limit feasible space of the robot manipulator. Therefore, exploiting efficient and large feasible region scheme is an important issue in robot motion planning areas.

Physical limits also always exist for a redundant robot manipulator in practice. In traditional pseudoinverse methods, it is difficult to consider joint limits obstacles. As is known that if the joint limits obstacles are not considered in the motion planning scheme, some generated joint solutions may go out of the safe area. The end-effector task may be failure since the joints with big values would be locked by the safe device or the manipulator would be damaged. To remedy this problem, our previous research considered joint limits avoidance as a bound constraint in a QP scheme, which could insure a safe operation for a redundant robot manipulator [27], [28].

To achieve the flexible obstacle avoidance of the WMRRM, a novel vector-based constrained obstacle avoidance (VOA) scheme is designed and analyzed in this article. The VOA scheme is applied to the WMRRM, which improves the flexibility of the redundant robot manipulator and the security of WMRRM in practical applications. Furthermore, the proposed VOA scheme can be extended to other mobile robot manipulator systems.

The remainder of this article is organized as follows. In Section II, the kinematic model of the WMRRM is given. Then, the obstacle avoidance constraint and physical limit constraint are designed, and these constraints are incorporated into the QP problem framework as the VOA scheme. In Section III, the VOA scheme, based on a QP problem framework, is converted equivalently into a piecewise linear projection equation (PLPE), and this PLPE is solved by a linear-variational-inequality-based primal–dual neural network (LVI-PDNN). Computer simulation experiments are carried out in Section IV to demonstrate the reliability of the VOA scheme. Finally, this article is summarized in Section V.

The motivation of this article is to design a flexible motion planning scheme to achieve the obstacle avoidance when the WMRRM system completes a complex end-effector task and the main contributions of this article are listed as follows.

1) A novel VOA scheme is designed and analyzed for motion planning of the WMRRM. This is the first time to propose a vector-based scheme applied to the WMRRM for the obstacle avoidance.
2) The proposed VOA scheme is more effective, accurate, and safe than traditional methods. This scheme makes better use of the redundancy of the redundant robot manipulator, effectively extends the feasible region of solutions, and greatly improves the flexibility of the WMRRM.
3) Detailed theoretical analysis and comparative simulation experiments are given to verify the advantages of the VOA scheme compared with the traditional obstacle avoidance methods.

II. Design of the Control Scheme

First, the overall kinematic model of the WMRRM is established. Then, the obstacle avoidance constraint and physical limit constraint are discussed. In the end, all the aforementioned constraints are incorporated into the QP problem framework as the VOA scheme.

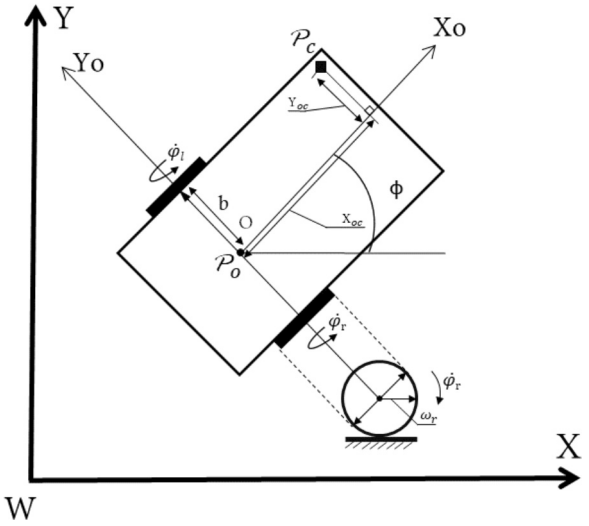

Fig. 2. Geometric model of the mobile platform (the wheelchair).

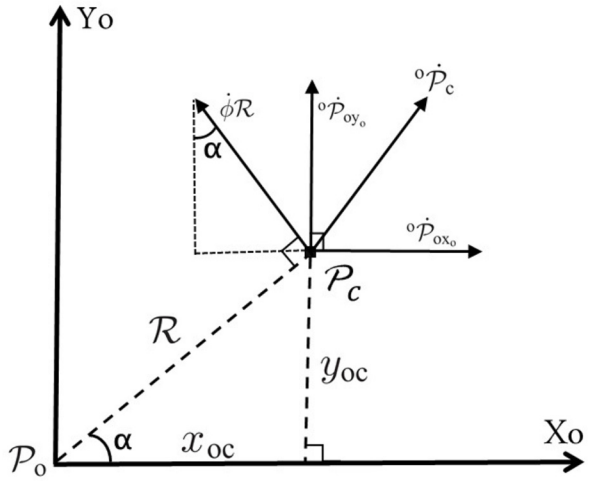

Fig. 3. Velocity of point $\mathcal{P}_c$ in the wheelchair coordinate system O.

A. Kinematic Model of the WMRRM

The kinematic dynamic model of the WMRRM is given at the velocity level as

$$\mathcal{J}_W\dot{\theta} = \dot{\mathcal{R}}_w \tag{1}$$

where $\mathcal{J}_W \in \mathbb{R}^{m\times n}$ denotes the Jacobian matrix of the WMRRM. For the WMRRM, the end effector works in a 3-D space and the system has eight actuators, and thus $m = 3$ and $n = 8$. $\dot{\theta} \in \mathbb{R}^n$ is a vector which comprises six joint velocities of the redundant robot manipulator and two rotation velocities of driving wheels of the mobile platform. $\dot{\mathcal{R}}_W$ denotes the velocity vector of the end effector.

The following four coordinate systems are defined and they are shown in Fig. 2.

W: The coordinate system of the workspace of the WMRRM.

O: The coordinate system whose origin is point $\mathcal{P}_o$ which is the midpoint of the line connecting the driving wheels.

C: The coordinate system fixed at point $\mathcal{P}_c$ on the wheelchair.

E: The coordinate system of the end effector of the WMRRM.

The kinematic model of the redundant robot manipulator can be obtained by its D-H model, i.e.,

$$\begin{aligned}{}^c\mathcal{P}_E &= {}^c_1\mathcal{T}\cdot{}^1_2\mathcal{T}\cdot{}^2_3\mathcal{T}\cdot{}^3_4\mathcal{T}\cdot{}^4_5\mathcal{T}\cdot{}^5_6\mathcal{T}\cdot{}^6\mathcal{P}_E \\ &= {}^c_6\mathcal{T}\cdot{}^6\mathcal{P}_E\end{aligned}$$

where ${}^c\mathcal{P}_E \in \mathbb{R}^{m+1}$ represents the end-effector position vector of the WMRRM in the coordinate system C. ${}^c_1\mathcal{T}$, ${}^1_2\mathcal{T}$, ${}^2_3\mathcal{T}$, ${}^3_4\mathcal{T}$, ${}^4_5\mathcal{T}$, and ${}^5_6\mathcal{T}$ are the homogeneous transform matrices to describe the spatial relationship between two adjacent links of the redundant robot manipulator. Then, the kinematic model of the WMRRM can be acquired

$$\begin{bmatrix}\mathcal{R}_W \\ \mathbf{1}\end{bmatrix} = {}^w_c\mathcal{T}\cdot{}^c\mathcal{P}_E \tag{2}$$

where ${}^w_c\mathcal{T}$ denotes the transform matrix of mobile platform from coordinate system C to coordinate system W. ${}^w_c\mathcal{T}$ can be acquired from the geometric model of the mobile platform which is shown in Fig. 2. Some symbols are defined in Fig. 2 and other mathematical symbols are defined as follows.

$\mathcal{P}_o$*:* The midpoint of the line connecting the driving wheels and its coordinates are $(x_{\rm wo}, y_{\rm wo}, z_{\rm wo})$ in the coordinate system W.

$\mathcal{P}_c$*:* The install location of the redundant robot manipulator on the wheelchair. Its coordinate is $(x_{\rm wc}, y_{\rm wc}, z_{\rm wc})$ in the coordinate system W and $(x_{\rm oc}, y_{\rm oc}, z_{\rm oc})$ in the coordinate system O. Note that these parameters are constant.

b: The distance between $\mathcal{P}_o$ and the driving wheels.

w_r*:* The radius of driving wheels.

ϕ*:* The heading angle of the WMRRM and shown in Fig. 2.

$\dot{\varphi}_l, \dot{\varphi}_r$*:* Rotation velocities of driving wheels.

Considering $\mathcal{P}_o$ in the coordinate system O, we have

$$\begin{aligned}{}^o\dot{\mathcal{P}}_o &= \begin{bmatrix}{}^o\dot{\mathcal{P}}_{ox_o} \\ {}^o\dot{\mathcal{P}}_{oy_o} \\ {}^o\dot{\mathcal{P}}_{oz_o}\end{bmatrix} = \begin{bmatrix}\frac{w_r}{2}\dot{\varphi}_l + \frac{w_r}{2}\dot{\varphi}_r \\ 0 \\ 0\end{bmatrix} \\ \dot{\phi} &= -\frac{w_r}{2b}\dot{\varphi}_l + \frac{w_r}{2b}\dot{\varphi}_r = \begin{bmatrix}-\frac{w_r}{2b} & \frac{w_r}{2b}\end{bmatrix}\begin{bmatrix}\dot{\varphi}_l \\ \dot{\varphi}_r\end{bmatrix}\end{aligned} \tag{3}$$

where ${}^o\dot{\mathcal{P}}_o$ represents the velocity of point $\mathcal{P}_o$ in the coordinate system O. ${}^o\dot{\mathcal{P}}_{ox_o}$, ${}^o\dot{\mathcal{P}}_{oy_o}$, and ${}^o\dot{\mathcal{P}}_{oz_o}$ represent the velocity components on the axis, respectively.

According to Fig. 3, the linear speed of point $\mathcal{P}_c$ perpendicular to $O\mathcal{P}_c$ is $\dot{\phi}\mathcal{R}$. In addition, the velocity of point $\mathcal{P}_c$ in the coordinate system O is

$${}^o\dot{\mathcal{P}}_c = \begin{bmatrix}{}^o\dot{\mathcal{P}}_{cx_o} \\ {}^o\dot{\mathcal{P}}_{cy_o} \\ {}^o\dot{\mathcal{P}}_{cz_o}\end{bmatrix} = \begin{bmatrix}{}^o\dot{\mathcal{P}}_{ox_o} - \dot{\phi}\mathcal{R}\sin\alpha \\ {}^o\dot{\mathcal{P}}_{oy_o} + \dot{\phi}\mathcal{R}\cos\alpha \\ {}^o\dot{\mathcal{P}}_{oz_o}\end{bmatrix} \tag{4}$$

where ${}^o\dot{\mathcal{P}}_c$ represents the velocity of point $\mathcal{P}_c$ in the coordinate system O, and ${}^o\dot{\mathcal{P}}_{cx_o}$, ${}^o\dot{\mathcal{P}}_{cy_o}$, and ${}^o\dot{\mathcal{P}}_{cz_o}$ represent the velocity components on the axis, respectively.

According to the geometry relationship shown in Fig. 3, we have $\mathcal{R}\sin\alpha = y_{\rm oc}$ and $\mathcal{R}\cos\alpha = x_{\rm oc}$. Substituting (3)

into (4), we have

$$
\begin{aligned}
{}^{o}\dot{\mathcal{P}}_c &= \begin{bmatrix} {}^{o}\dot{\mathcal{P}}_{\mathrm{cx}_o} \\ {}^{o}\dot{\mathcal{P}}_{\mathrm{cy}_o} \\ {}^{o}\dot{\mathcal{P}}_{\mathrm{cz}_o} \end{bmatrix} \\
&= \begin{bmatrix} \left(\frac{w_r}{2} + \frac{w_r}{2b} y_{\mathrm{oc}}\right)\dot{\varphi}_l + \left(\frac{w_r}{2} - \frac{w_r}{2b} y_{\mathrm{oc}}\right)\dot{\varphi}_r \\ -\frac{w_r}{2b} x_{\mathrm{oc}}\dot{\varphi}_l + \frac{w_r}{2b} x_{\mathrm{oc}}\dot{\varphi}_r \\ 0 \end{bmatrix}.
\end{aligned}
$$

By multiplying a rotation transform matrix, we can convert the velocity of point $\mathcal{P}_c$ from the coordinate system O to the coordinate system W, i.e.,

$$
\begin{bmatrix} {}^{w}\dot{\mathcal{P}}_{\mathrm{cx}} \\ {}^{w}\dot{\mathcal{P}}_{\mathrm{cy}} \end{bmatrix} = \begin{bmatrix} \cos\phi & -\sin\phi \\ \sin\phi & \cos\phi \end{bmatrix} \begin{bmatrix} \frac{w_r}{2} + \frac{w_r}{2b} y_{\mathrm{oc}} & \frac{w_r}{2} - \frac{w_r}{2b} y_{\mathrm{oc}} \\ -\frac{w_r}{2b} x_{\mathrm{oc}} & \frac{w_r}{2b} x_{\mathrm{oc}} \end{bmatrix} \begin{bmatrix} \dot{\varphi}_l \\ \dot{\varphi}_r \end{bmatrix}
$$

$$
{}^{w}\dot{\mathcal{P}}_{\mathrm{cz}} = 0
$$

where ${}^{o}\dot{\mathcal{P}}_{\mathrm{cx}_o}$, ${}^{o}\dot{\mathcal{P}}_{\mathrm{cy}_o}$, and ${}^{o}\dot{\mathcal{P}}_{\mathrm{cz}_o}$ represent the velocity components on the axis, respectively, in the coordinate system W.

By integrating ${}^{w}\dot{\mathcal{P}}_c$ and $\dot{\phi}$, we have

$$
{}^{w}\mathcal{P}_c = \begin{bmatrix} x_{\mathrm{wc}} \\ y_{\mathrm{wc}} \\ z_{\mathrm{wc}} \end{bmatrix} = \int {}^{w}\dot{\mathcal{P}}_c = \begin{bmatrix} \int {}^{w}\dot{\mathcal{P}}_{\mathrm{cx}} + x_{\mathrm{wc}}(0) \\ \int {}^{w}\dot{\mathcal{P}}_{\mathrm{cy}} + y_{\mathrm{wc}}(0) \\ \int {}^{w}\dot{\mathcal{P}}_{\mathrm{cz}} + z_{\mathrm{wc}}(0) \end{bmatrix}
$$

$$
\phi = \int \dot{\phi} + \phi(0).
$$

Once x_{wc}, y_{wc}, and z_{wc} are obtained, the homogeneous transform matrix ${}^{w}_{c}\mathcal{T}$ can be obtained as follows:

$$
{}^{w}_{c}\mathcal{T} = \begin{bmatrix} \cos\phi & -\sin\phi & 0 & x_{\mathrm{wc}} \\ \sin\phi & \cos\phi & 0 & y_{\mathrm{wc}} \\ 0 & 0 & 1 & z_{\mathrm{wc}} \\ 0 & 0 & 0 & 1 \end{bmatrix}.
$$

After the above deduction, the overall kinematic model of the WMRRM can be obtained from (2). The Jacobian matrix $\mathcal{J}_W$ can be calculated as

$$
\mathcal{J}_W = \frac{\partial \mathcal{R}_W}{\partial \theta}.
$$

In order to obtain the resolution of (1), the following QP problem can be applied [22], i.e.,

$$
\text{minimize} \quad \frac{1}{2}\dot{\theta}^T\dot{\theta} \tag{5}
$$

$$
\text{subject to} \quad \mathcal{J}_W\dot{\theta} = \dot{\mathcal{R}}_W. \tag{6}
$$

B. Obstacle Avoidance Constraint

The obstacle avoidance scheme will be formulated as an inequality constraint and incorporated directly into the QP problem (5) and (6).

1) Traditional Scheme I: Obstacle avoidance can be seen as the critical point on the robot manipulator must keep a certain distance from the obstacle point. As shown in Fig. 4, we define the point which is the nearest point to the obstacle point $\mathcal{O}$ on the vulnerable link L_i of the robot manipulator or its extended line as the critical point $\mathcal{C}$. In order to avoid obstacles, it is necessary to compute the distance between point $\mathcal{C}$ and point $\mathcal{O}$, and then give the critical point $\mathcal{C}$ an escape velocity away from the obstacle point $\mathcal{O}$. Then, the robot manipulator will keep away from the obstacles [22], [29].

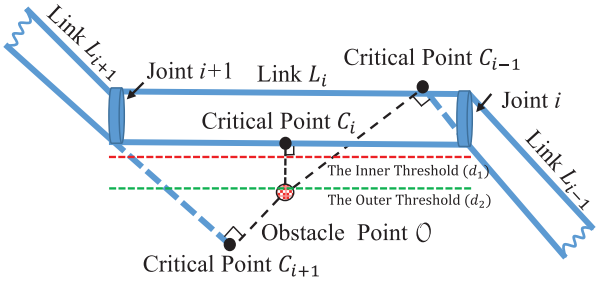

Fig. 4. Obstacle point $\mathcal{O}$ and the critical point $\mathcal{C}_i$ on the vulnerable link L_i.

An intuitionistic idea is that the manipulator can continue to work when the manipulator does not meet the obstacle point, otherwise the manipulator should stop or escape in the opposite direction. This is termed traditional scheme I. This scheme can be described as an inequality in mathematics, i.e.,

$$
\mathcal{J}_o\dot{\theta} \leq \mathbf{0} \tag{7}
$$

where $\mathcal{J}_o \in \mathbb{R}^{m\sigma\times n}$. σ represents the pairs of point $\mathcal{O}$ and point $\mathcal{C}$. $\mathcal{J}_o$ is defined as

$$
\mathcal{J}_o = -\overrightarrow{\mathcal{R}_{\mathrm{oc}}} \diamond \mathcal{J}_c(\theta)
$$

where the operator $\diamond$ is defined as $\mathbf{x} \diamond \mathbf{y} = [x_1y_1, x_2y_2, \ldots, x_\ell y_\ell]^T$ with $\mathbf{x} = [x_1, x_2, \ldots, x_\ell]^T$ being a column vector and $\mathbf{y} = [y_1, y_2, \ldots, y_\ell]^T$ being a matrix. $\mathcal{J}_c \in \mathbb{R}^{m\sigma\times n}$ denotes the Jacobian matrix of critical point $\mathcal{C}$ and $\overrightarrow{\mathcal{R}_{\mathrm{oc}}}$ is

$$
\overrightarrow{\mathcal{R}_{\mathrm{oc}}} = \mathrm{sgn}\left[\, x_c - x_o,\ y_c - y_o,\ z_c - z_o \,\right]^T
$$

where (x_c, y_c, z_c) is the coordinate of point $\mathcal{C}$ and (x_o, y_o, z_o) is the coordinate of point $\mathcal{O}$, and sgn[$\cdot$] represents a scalar signum function, i.e.,

$$
\mathrm{sgn}[\ \iota\ ] = \begin{cases} 1, & \text{if } \iota > 0 \\ 0, & \text{if } \iota = 0 \\ -1, & \text{if } \iota < 0. \end{cases}
$$

2) Traditional Scheme II: In traditional scheme I (7), the WMRRM will avoid obstacles only when the distance between point $\mathcal{O}$ and point $\mathcal{C}$ is zero, which may cause the emergency stop of the WMRRM. Therefore, parameter ν can replace $\mathbf{0}$ in (7) to avoid the emergency stop of the WMRRM [22], [29], i.e.,

$$
\mathcal{J}_o\dot{\theta} \leq \nu \tag{8}
$$

where $\nu \in \mathbb{R}^3$ is

$$
\nu = \mathcal{S}(d)\max\left\{\mathcal{J}_o\dot{\theta}|_{d=d_2}, \mathbf{0}\right\}
$$

with the operator max{$\mathbf{b}$, $\mathbf{0}$} being the vector-valued function for the maximal values between components b_i and 0 [22], [29] and the smooth function $\mathcal{S}(\cdot)$ is defined as

$$
\mathcal{S}(d) = \begin{cases} 1, & \text{if } d \geq d_2 \\ \sin^2\left(\frac{\pi}{2} \cdot \frac{d-d_1}{d_2-d_1}\right), & \text{if } d_1 < d < d_2 \\ 0, & \text{if } d \leq d_1 \end{cases}
$$

where d represents the distance between point $\mathcal{C}$ and point $\mathcal{O}$. As shown in Fig. 4, d_1 is the inner threshold and d_2 is the outer threshold.

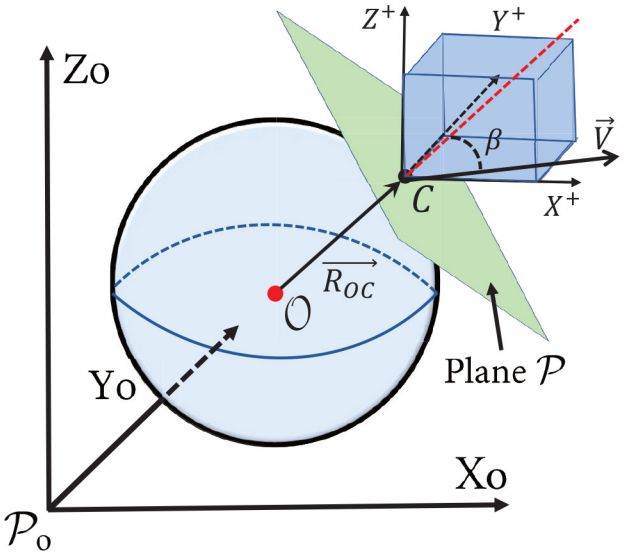

Fig. 5. Feasible space of obstacle avoidance schemes.

3) Shortages of Traditional Schemes I and II: As shown in Fig. 5, the feasible spaces of the solutions to traditional schemes I and II are only the first quadrant in coordinate system $X^+Y^+Z^+$. That is to say, the feasible space is not fully utilized. The reason is as follows. When the distance between point $\mathcal{O}$ and point $\mathcal{C}$ is the minimum constraint distance between point $\mathcal{O}$ and point $\mathcal{C}$, the obstacle avoidance scheme (7) starts to work and $\overrightarrow{\mathcal{R}_{\text{oc}}}$ satisfies

$$\begin{aligned}\overrightarrow{\mathcal{R}_{\text{oc}}} &= \text{sgn}\big[x_c - x_o,\ y_c - y_o,\ z_c - z_o\big]^T \\ &= [+1, +1, +1]^T.\end{aligned}$$

By substituting (9) into (7), the feasible space is calculated and shown in Fig. 5. The feasible space of traditional scheme I is composed of points in the first quadrant of the coordinate system with point $\mathcal{C}$ as the origin and X^+, Y^+, and Z^+ as the coordinate axes, just like the blue space in Fig. 5. A similar problem exists with traditional scheme II. In practical applications, the limited feasible space may generate unreasonable solutions. This may lead to obstacle avoidance failure.

An ideal feasible space is the outward space of tangent plane $\mathcal{P}$ as shown in Fig. 5. It can be seen that the feasible space obtained by the traditional scheme is much smaller than the ideal feasible space. In other words, the traditional scheme is not flexible enough to make full use of the redundancy of the redundant manipulator.

4) Improved Obstacle Avoidance Constraint: We proposed a new vector-based scheme to make full use of the ideal feasible space, i.e.,

$$\tilde{\mathcal{J}}_o\dot{\theta} \le \tilde{\nu} \tag{9}$$

where $\tilde{\mathcal{J}}_o$ and $\tilde{\nu}$ are defined as

$$\begin{aligned}\tilde{\mathcal{J}}_o &= -\overrightarrow{\tilde{\mathcal{R}}_{\text{oc}}} \cdot \mathcal{J}_c(\theta) \\ \tilde{\nu} &= \mathcal{S}(d)\max\left\{\tilde{\mathcal{J}}_o\dot{\theta}|_{d=d_2}, 0\right\}\end{aligned}$$

with $\overrightarrow{\tilde{\mathcal{R}}_{\text{oc}}} = \overrightarrow{\mathcal{R}_{\text{oc}}}^T$ and $\overrightarrow{\mathcal{V}}$ being the velocity vector of point $\mathcal{C}$, which is the critical point of the manipulator. We can extend the left-hand side of (9) as

$$\tilde{\mathcal{J}}_o\dot{\theta} = -\overrightarrow{\tilde{\mathcal{R}}_{\text{oc}}} \cdot \mathcal{J}_c\dot{\theta} = -\overrightarrow{\tilde{\mathcal{R}}_{\text{oc}}} \cdot \overrightarrow{\mathcal{V}}.$$

According to the vector multiplication rule, $\overrightarrow{\tilde{\mathcal{R}}_{\text{oc}}} \cdot \overrightarrow{\mathcal{V}} = |\overrightarrow{\tilde{\mathcal{R}}_{\text{oc}}}| \cdot |\overrightarrow{\mathcal{V}}| \cos\beta$. If $\overrightarrow{\tilde{\mathcal{R}}_{\text{oc}}} \cdot \overrightarrow{\mathcal{V}} \ge 0$, we can conclude that the angle between the vectors $\overrightarrow{\tilde{\mathcal{R}}_{\text{oc}}}$ and $\overrightarrow{\mathcal{V}}$ is less than or equal to 90°. This means that point $\mathcal{C}$ can be the out side of the plane $\mathcal{P}$ or on the plane $\mathcal{P}$. In other words, the VOA scheme makes it possible to make full use of the ideal feasible space.

C. Physical Limits Avoidance Constraint

Physical limits are common problems for the practice robot system. It is necessary to consider joint limits to ensure the safety of the manipulator. These limits can be described as the following inequalities, i.e.,

$$\theta^- \le \theta \le \theta^+, \dot{\theta}^- \le \dot{\theta} \le \dot{\theta}^+ \tag{10}$$

where $\theta^\pm$ and $\dot{\theta}^\pm$ denote the limits of joint angles and joint velocities of robot manipulator, respectively. According to [27], (10) can be converted into a bound constraint, i.e.,

$$\eta^- \le \dot{\theta} \le \eta^+ \tag{11}$$

where $\eta^- = \max\{p(\theta^- - \theta), \dot{\theta}^-\} \in \mathbb{R}^n$ and $\eta^+ = \min\{p(\theta^+ - \theta), \dot{\theta}^+\} \in \mathbb{R}^n$. Parameter p is a positive number. Then, we should incorporate the boundary constraint (11) into the control scheme.

D. VOA Scheme

By incorporating the inequality constraint (9) and the boundary constraint (11) into a QP problem, the VOA scheme for the WMRRM is formulated as

$$\begin{aligned}\text{minimize}\quad & \frac{1}{2}\dot{\theta}^T\dot{\theta} && (12)\\ \text{subject to}\quad & \mathcal{J}_W\dot{\theta} = \dot{\mathcal{R}}_W && (13)\\ & \tilde{\mathcal{J}}_o\dot{\theta} \le \tilde{\nu} && (14)\\ & \eta^- \le \dot{\theta} \le \eta^+. && (15)\end{aligned}$$

III. LVI-Based Primal–Dual Neural Network

The VOA scheme based on a QP problem framework, can be converted equivalently into a PLPE [30], then this PLPE is solved by LVI-PDNN.

Theorem 1 (VOA-PLPE Conversion): The VOA scheme (12)–(15), which is based on the QP problem with equality, inequality, and bound constraints can be transformed into the following PLPE [30], i.e.,

$$P_\Omega(\chi - (\mathcal{M}\chi + q)) - \chi = 0 \tag{16}$$

where $P_\Omega(\cdot)$ is a piecewise-linear projection operator. $\chi = [\dot{\theta},\ \mu_e,\ \mu_i]^T \in \mathbb{R}^{n+m+m\sigma}$ is the primal–dual decision variable vector. $\mu_e \in \mathbb{R}^m$ and $\mu_i \in \mathbb{R}^{m\sigma}$ are the dual decision variable vectors for equality (13) and inequality (14), respectively. The

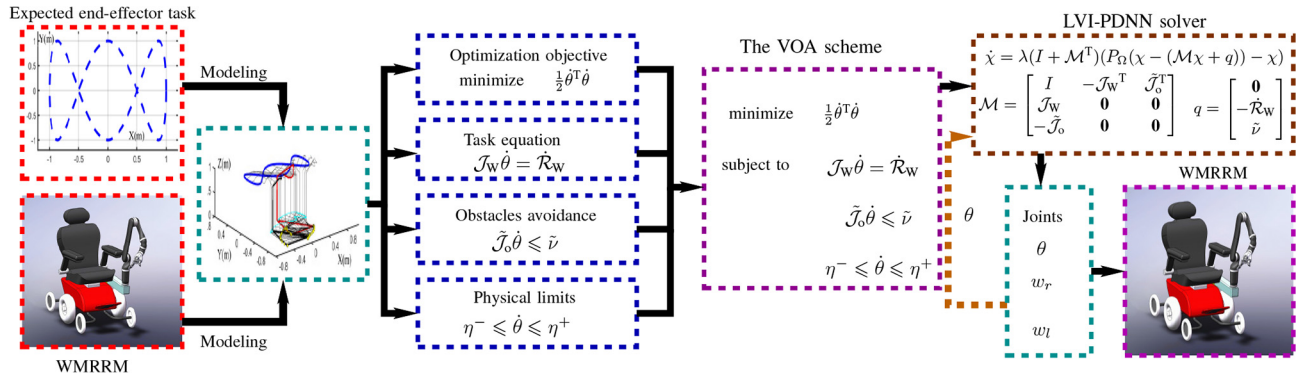

Fig. 6. Framework of the VOA scheme for solving the motion planning problem of WMRRM.

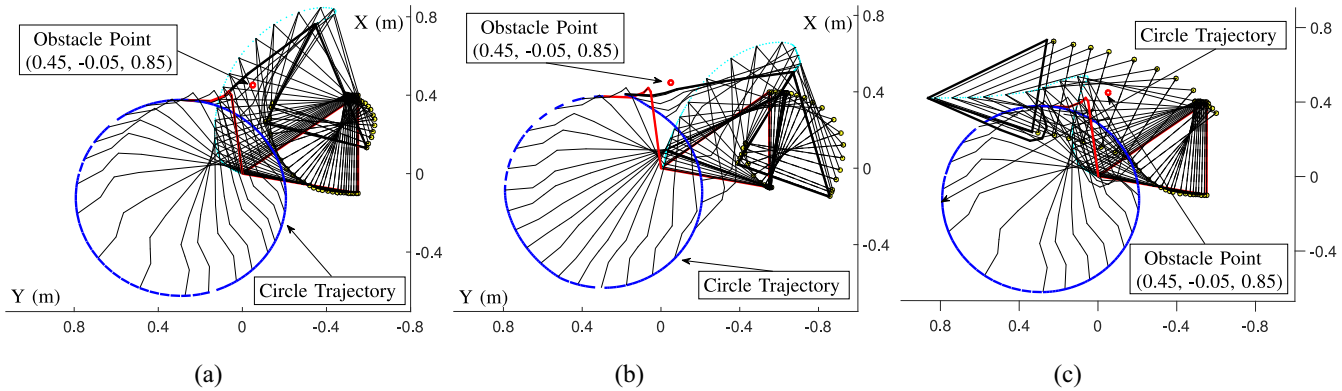

Fig. 7. Tracking trajectories and obstacle points synthesized by WOA, TOA, and VOA schemes. Yellow dots indicate the track of the driving wheels, the red line indicates the initial state, black lines indicate the track of the WMRRM, and the most thick one indicates the final state. (a) WOA scheme. (b) TOA scheme. (c) VOA scheme.

convex set Ω is defined as

$$\Omega = \left\{\chi \in \mathbb{R}^{m+n+m\sigma} | \chi^{-} \leq \chi \leq \chi^{+}\right\}$$

$$\text{with } \chi^{-} = \begin{bmatrix} \eta^{-} \\ -\varpi l_e \\ \mathbf{0} \end{bmatrix} \quad \text{and } \chi^{+} = \begin{bmatrix} \eta^{+} \\ \varpi l_e \\ \varpi l_i \end{bmatrix}$$

where $l_e := [1, 1, \ldots, 1]^T \in \mathbb{R}^m$, $l_i := [1, 1, \ldots, 1]^T \in \mathbb{R}^{m\sigma}$, and $\varpi \gg 0$ denotes a huge number that can replace $+\infty$. Vector $q \in \mathbb{R}^{n+m+m\sigma}$ and matrix $\mathcal{M} \in \mathbb{R}^{(n+m+m\sigma)\times(n+m+m\sigma)}$ are

$$\mathcal{M} = \begin{bmatrix} I & -\mathcal{J}_W{}^T & \tilde{\mathcal{J}}_o^T \\ \mathcal{J}_W & \mathbf{0} & \mathbf{0} \\ -\tilde{\mathcal{J}}_o & \mathbf{0} & \mathbf{0} \end{bmatrix}, \quad \text{and } q = \begin{bmatrix} \mathbf{0} \\ -\dot{\mathcal{R}}_W \\ \tilde{\nu} \end{bmatrix}.$$

Proof: See [30, Sec. 3]. ■

Through our previous neural network design method [28], [31], an LVI-PDNN can be applied to solve the PLPE problem (16), i.e.,

$$\dot{\chi} = \lambda\big(I + \mathcal{M}^T\big)\{P_{\Omega}(\chi - (\mathcal{M}\chi + q)) - \chi\} \tag{17}$$

where parameter λ is a parameter related to the convergence rate [31] and the global convergence of LVI-PDNN was proved in [28, Th. 3].

The framework of the proposed VOA scheme is shown as Fig. 6 and the overall design steps of the proposed VOA scheme are presented as follows.

Step 1: According to requirements of the end-effector task and the practical WMRRM system, the trajectories of the end effector of the WMRRM and parameters $\theta(0)$, $\theta^{\pm}$, $\dot{\theta}^{\pm}$ are determined.

Step 2: Based on the trajectories and parameters of the practical WMRRM system in step 1, the kinematic model of the whole system is established.

Step 3: According to the coordinates of the obstacles in the coordinate system W, the location of critical points of the WMRRM and parameters d_1 and d_2 are determined.

Step 4: The optimization objective, the equality constraint (i.e., control task equation), and inequality constraints (i.e., obstacle avoidance and physical limits) for achieving the end-effector control task (i.e., the control task of the end effector) and secondary tasks (i.e., the obstacle avoidance task and physical limits avoidance task) are designed as a time-varying QP scheme.

Step 5: According to the design formula of LVI-PDNN (17) in the revised manuscript, the recurrent neural network for solving the QP problem in step 4 is formed and the parameter λ is determined.

Step 6: Synthesized by the LVI-PDNN in step 5, the angles of joints and wheels are obtained, and then put into the practical WMRRM system for achieving the obstacle avoidance.

IV. Computer Simulation Verifications

Two comparison simulation experiments of three schemes are conducted in this section.

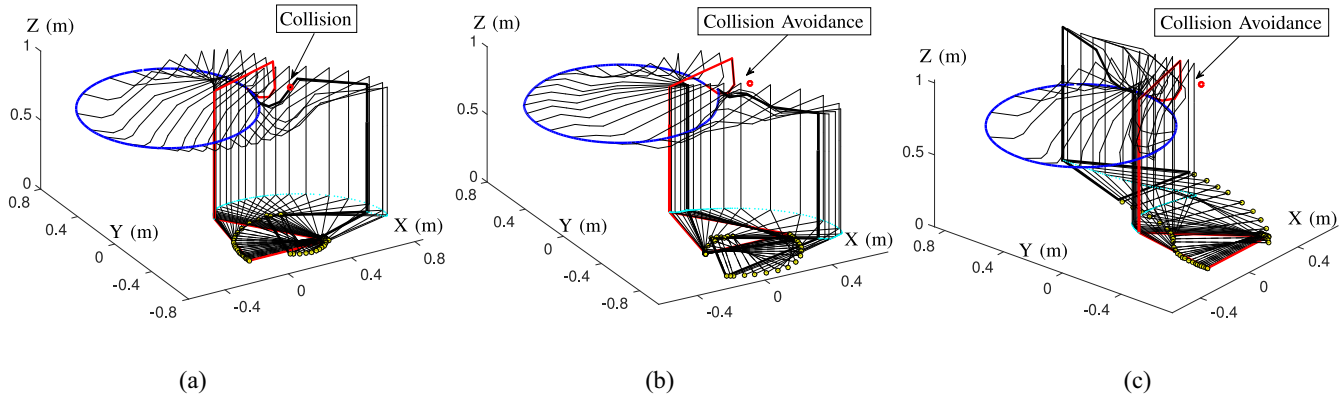

Fig. 8. Comparative simulations of 3-D tracking trajectories of WOA, TOA, and VOA schemes. (a) WOA scheme. (b) TOA scheme. (c) VOA scheme.

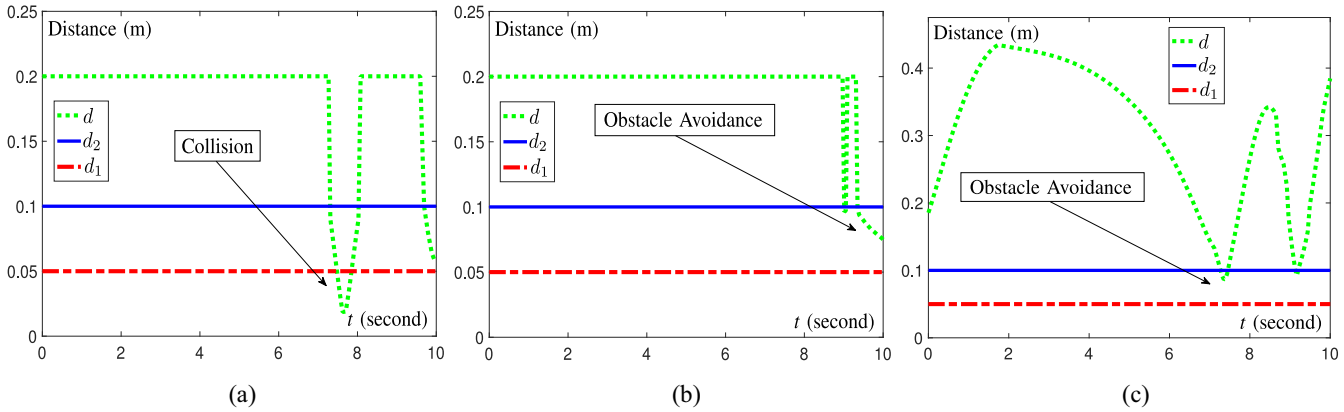

Fig. 9. Minimum distances between obstacle point and critical point of WOA, TOA, and VOA schemes. (a) WOA scheme. (b) TOA scheme. (c) VOA scheme.

1) Scheme without considering obstacle avoidance (WOA) (i.e., $\tilde{\mathcal{J}}_o = \mathbf{0}$) [32].
2) Traditional obstacle avoidance II (TOA-II) scheme [22], [29].
3) VOA scheme.

For comparisons, the above WOA, TOA, and VOA schemes are applied to the WMRRM and perform the same trajectory tracking task from the same initial state and avoid the same obstacle point. The experiments are finished with MATLAB R2016a. Specifically, in the ensuing simulations, $\beta = 1 \times 10^4$ in the LVI-PDNN model (17), the initial joint angle is set as $\theta(0) = [-1.46\pi,\ 1.44\pi,\ 0.48\pi,\ 1.27\pi,\ 0.58\pi,\ 0.77\pi\ ]^T$ rad. The inner and outer safe thresholds d_1 and d_2 in smooth function $\mathcal{S}(d)$ (9) are set as $d_1 = 0.05$ m and $d_2 = 0.10$ m.

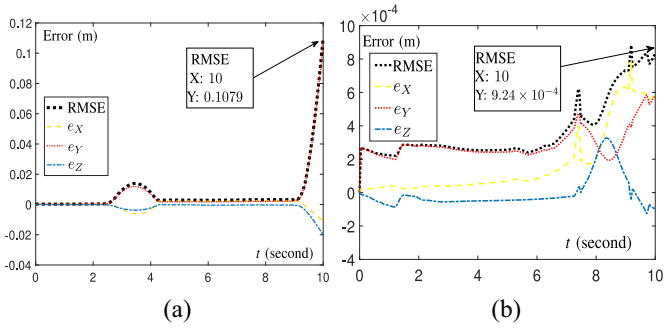

Fig. 10. Position errors of end effectors of simulative experiment among TOA and VOA schemes. (a) TOA scheme. (b) VOA scheme.

A. Comparative Simulation Experiment I: Circle Trajectory

The desired path of the tracking experiment is a circle with a radius of 0.5 m in a plane of $z = 0.7$ m. The coordinate of the obstacle point $\mathcal{O}$ is $(0.45,\ -0.05,\ 0.85)$ m, which is close to the desired path in the world coordinate system W. The simulation results of WOA, TOA, and VOA schemes are shown in Figs. 7–10.

First, the tracking trajectory and distance of $\mathcal{OC}$ are shown in Figs. 7–9. As can be seen from Fig. 7, all of these three schemes track the desired path (i.e., a circle). However, as shown in Fig. 8, the manipulator collides with the obstacle. This means that the tracking task synthesized by the WOA scheme is failed. That is to say, if a scheme does not consider the obstacle avoidance constraint, it cannot be applied to practical applications. In contrast, with the TOA scheme and the proposed VOA scheme, the manipulator avoids the obstacle successfully. This result can be further confirmed in Fig. 9. Fig. 9(a) shows that the minimum distance d of the WOA scheme is less than the inner threshold d_1. This means that it is difficult for the WOA scheme to avoid the obstacle due to the adjacent location of the obstacle. Contrastively,

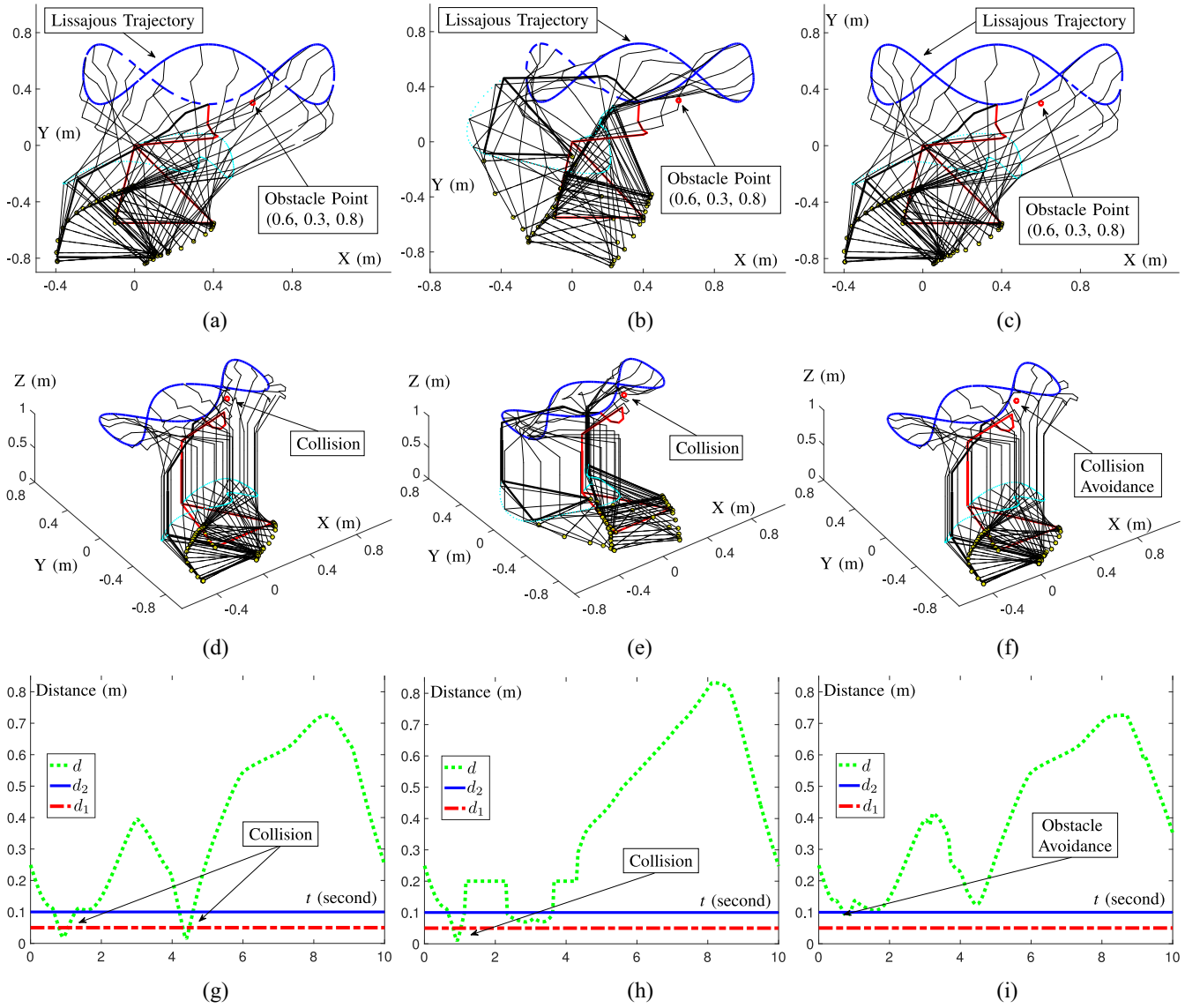

Fig. 11. Comparative simulations among WOA, TOA, and VOA schemes. Yellow dots indicate the driving wheel in (a)–(f). The red line indicates the initial state in (a)–(f). Black lines indicate the track of the WMRRM and the most thick one indicates the final state in (a)–(f). (a)–(c) Tracking trajectories and obstacle points. (d)–(f) 3-D tracking trajectories. (g)–(i) Minimum obstacle-critical point distances. (a), (d), and (g) WOA scheme. (b), (e), and (h) TOA scheme. (c), (f), and (i) VOA scheme.

in Fig. 9(b) and (c), since the minimum distance d is always larger than the inner threshold d_1, the TOA and VOA schemes become agile and avoid collision in the same situation. These comparisons results show that the schemes with obstacle avoidance constraint are effective.

Second, end-effector position errors of three schemes when executing tracking tasks are shown in Fig. 10. From Fig. 10(a), we see that the position errors of the TOA scheme during the task execution period are very large, i.e., about 10^{-1} m level. This means that even the TOA scheme can avoid the obstacle, it still cannot be applied to practical applications due to its large position errors. In contrast, from Fig. 10(b), we can see quite evidently that the proposed VOA scheme can complete the obstacle avoidance task successfully with a tiny position errors (i.e., only about 10^{-4} m). These simulation results demonstrate that the proposed VOA scheme is accurate and can be applied widely.

TABLE I
CALCULATING TIME OF THE WOA SCHEME, TOA SCHEME, AND VOA SCHEME FOR TEN CONSECUTIVE EXPERIMENTS

Algorithms	WOA scheme	TOA scheme	VOA scheme
No.1	8.977 s	32.480 s	7.738 s
No.2	9.188 s	32.755 s	7.931 s
No.3	8.842 s	34.484 s	7.591 s
No.4	8.576 s	35.478 s	8.484 s
No.5	8.665 s	35.999 s	8.530 s
No.6	8.714 s	36.419 s	8.691 s
No.7	9.270 s	36.794 s	8.567 s
No.8	8.661 s	37.761 s	8.143 s
No.9	8.300 s	35.808 s	8.721 s
No.10	8.960 s	37.536 s	8.180 s
Average	8.8153 s	35.5514 s	8.2576 s

Third, the calculating time of the aforementioned three schemes are shown in Table I. This table contains the results of ten consecutive experiments of each scheme. From these

data, we can see that the calculating time of the proposed VOA scheme is much shorter than the TOA scheme, which verifies the superiority of our proposed VOA scheme. It is worth pointing out that compared with the WOA scheme, the calculating time of the VOA scheme is still shorter. This result further shows that the proposed VOA scheme is very efficient.

In summary, the above comparative simulations illustrate that the VOA scheme is more effective, more accurate, safer, more efficient, and more widely applicable compared with the state-of-the-art schemes, i.e., WOA and TOA schemes.

B. Comparative Simulation Experiment II: Lissajous Trajectory

In this section, a more complex curve is tracked in this section, i.e., a Lissajous path in a plane of $z = 0.7$ m. The tracking trajectories and the obstacle points are shown in Fig. 11(a)–(c). The coordinates of obstacle point $\mathcal{O}$ is (0.6, 0.3, 0.8) m in the world coordinate system W. Other parameters setting are consistent with the tracking experiment one.

From Fig. 11(d)–(f), we can see that in such a complex twisted trajectory, both of the WOA and TOA schemes collide with the obstacle points, which means that the traditional obstacle avoidance schemes would lose efficacy if the obstacles are very close to the manipulator or the end-effector path is complex. Fig. 11(g) and (h) shows that the minimum distances d of WOA and TOA schemes are less than d_1 in this situation. It demonstrates the robot manipulator synthesized by the WOA scheme or TOA scheme cannot complete the end-effector task when the obstacles are very close to the expected path. In other words, the TOA scheme is not suitable for the tasks with complex trajectories with very close obstacles. In contrast, even if the desired path is as complex as the twisted line in Fig. 11(c) and the obstacles are very close to the manipulator, with the proposed VOA scheme, the obstacle avoidance can be achieved.

The above comparison simulations further demonstrate that the VOA scheme is more effective, more accurate, and safer.

V. Conclusion

In this article, a novel VOA scheme has been proposed and exploited to achieve the flexible obstacle avoidance of the WMRRM. In the VOA scheme, the obstacle avoidance constraint and the physical limits constraint have been formulated as an inequality constraint and a bound constraint in a QP problem. Finally, the VOA scheme has been converted equivalently into a PLPE and solved by an LVI-PDNN. Comparative simulations of the WMRRM verify the effectiveness, accuracy, safety, and practicality of the proposed VOA scheme. Future research is that the proposed VOA scheme would be performed in a practical mobile robot manipulator system.

References

[1] Z. Li, W. Yuan, S. Zhao, Z. Yu, Y. Kang, and C. L. P. Chen, "Brain-actuated control of dual-arm robot manipulation with relative motion," *IEEE Trans. Cogn. Develop. Syst.*, vol. 11, no. 1, pp. 51–62, Mar. 2019.

[2] M. Hao, W. Cao, M. Wu, Z. Liu, and S. Li, "An initiative service method based on fuzzy analytical hierarchy process and context intention inference for drinking service robot," *IEEE Trans. Cogn. Develop. Syst.*, vol. 11, no. 2, pp. 221–233, Jun. 2019.

[3] Y. Liu *et al.*, "Motor-imagery-based teleoperation of a dual-arm robot performing manipulation tasks," *IEEE Trans. Cogn. Develop. Syst.*, vol. 11, no. 3, pp. 414–424, Sep. 2019.

[4] M. F. Corapsiz and K. Erenturk, "Trajectory tracking control and contouring performance of three-dimensional CNC," *IEEE Trans. Ind. Electron.*, vol. 63, no. 4, pp. 2212–2220, Apr. 2016.

[5] E. Venator, G. S. Lee, and W. Newman, "Hardware and software architecture of ABBY: An industrial mobile manipulator," in *Proc. IEEE Int. Conf. Autom. Sci. Eng.*, Madison, WI, USA, 2013, pp. 324–329.

[6] Y. Xu and R. P. Paul, "A robot compliant wrist system for automated assembly," in *Proc. IEEE Int. Conf. Robot. Autom.*, vol.3. Cincinnati, OH, USA, 1990, pp. 1750–1755.

[7] S. Yang, R. A. Maclachlan, and C. N. Riviere, "Manipulator design and operation of a six-degree-of-freedom handheld tremor-canceling microsurgical instrument," *IEEE/ASME Trans. Mechatronics*, vol. 20, no. 2, pp. 761–772, Apr. 2015.

[8] M. S. Moses, R. J. Murphy, M. D. M. Kutzer, and M. Armand, "Modeling cable and guide channel interaction in a high-strength cable-driven continuum manipulator," *IEEE/ASME Trans. Mechatronics*, vol. 20, no. 6, pp. 2876–2889, Dec. 2015.

[9] W. Chung, C. Rhee, Y. Shim, H. Lee, and S. Park, "Door-opening control of a service robot using the multifingered robot hand," *IEEE Trans. Ind. Electron.*, vol. 56, no. 10, pp. 3975–3984, Oct. 2009.

[10] Q. Wu, X. Wang, B. Chen, H. Wu, and Z. Shao, "Development and hybrid force/position control of a compliant rescue manipulator," *Mechatronics*, vol. 46, pp. 143–153, Oct. 2017.

[11] J. Serón, J. L. Martínez, A. Mandow, A. J. Reina, J. Morales, and A. J. García-Cerezo, "Automation of the arm-aided climbing maneuver for tracked mobile manipulators," *IEEE Trans. Ind. Electron.*, vol. 61, no. 7, pp. 3638–3647, Jul. 2014.

[12] Z. Zhang and Y. Zhang, "Variable joint-velocity limits of redundant robot manipulators handled by quadratic programming," *IEEE/ASME Trans. Mechatronics*, vol. 18, no. 2, pp. 674–686, Apr. 2013.

[13] Z. Zhang, S. Chen, and S. Li, "Compatible convex–nonconvex constrained QP-based dual neural networks for motion planning of redundant robot manipulators," *IEEE Trans. Control Syst. Technol.*, vol. 27, no. 3, pp. 1250–1258, May 2019.

[14] L. Sciavicco and B. Siciliano, "A solution algorithm to the inverse kinematic problem for redundant manipulators," *IEEE Trans. Robot. Autom.*, vol. 4, no. 4, pp. 403–410, Aug. 1988.

[15] A. A. Maciejewski and C. A. Klein, "Obstacle avoidance for kinematically redundant manipulators in dynamically varying environments," *Int. J. Robot. Res.*, vol. 4, no. 3, pp. 109–117, 1985.

[16] H. Ding and S. P. Chan, "A real-time planning algorithm for obstacle avoidance of redundant robots," *J. Intell. Robot. Syst.*, vol. 16, no. 3, pp. 229–243, 1996.

[17] L. Jin, Y. Zhang, S. Li, and Y. Zhang, "Modified ZNN for time-varying quadratic programming with inherent tolerance to noises and its application to kinematic redundancy resolution of robot manipulators," *IEEE Trans. Ind. Electron.*, vol. 63, no. 11, pp. 6978–6988, Nov. 2016.

[18] S. Zhang and Y. Xia, "Two fast complex-valued algorithms for solving complex quadratic programming problems," *IEEE Trans. Cybern.*, vol. 46, no. 12, pp. 2837–2847, Dec. 2016.

[19] Y. Xia and W. Xing, "Parametric Lagrangian dual for the binary quadratic programming problem," *J. Glob. Optim.*, vol. 61, no. 2, pp. 221–233, 2015.

[20] Z. Zhang, Y. Lin, S. Li, Y. Li, Z. Yu, and Y. Luo, "Tricriteria optimization-coordination motion of dual-redundant-robot manipulators for complex path planning," *IEEE Trans. Control Syst. Technol.*, vol. 26, no. 4, pp. 1345–1357, Jul. 2018.

[21] F. T. Cheng, Y. T. Lu, and Y. Y. Sun, "Window-shaped obstacle avoidance for a redundant manipulator," *IEEE Trans. Syst., Man, Cybern. B, Cybern.*, vol. 28, no. 6, pp. 806–815, Dec. 1998.

[22] Y. Zhang and J. Wang, "Obstacle avoidance for kinematically redundant manipulators using a dual neural network," *IEEE Trans. Syst., Man, Cybern. B, Cybern.*, vol. 34, no. 1, pp. 752–759, Feb. 2004.

[23] S. S. Ge and Y. J. Cui, "New potential functions for mobile robot path planning," *IEEE Trans. Robot. Autom.*, vol. 16, no. 5, pp. 615–620, Oct. 2000.

[24] W. Guan, Z. Weng, and J. Zhang, "Obstacle avoidance path planning for manipulator based on variable-step artificial potential method," in *Proc. Chinese Control Decis. Conf.*, Qingdao, China, pp. 4325–4329, 2015.

[25] J.-O. Kim and P. K. Khosla, "Real-time obstacle avoidance using harmonic potential functions," *IEEE Trans. Robot. Autom.*, vol. 8, no. 3, pp. 338–349, Jun. 1992.

[26] W. S. Tang, C. M. L. Lam, and J. Wang, "Kinematic control and obstacle avoidance for redundant manipulators using a recurrent neural network," in *Artificial Neural Networks—ICANN*, Heidelberg, Germany: Springer, 2001, pp. 922–929.
[27] Z. Zhang, Z. Li, Y. Zhang, Y. Luo, and Y. Li, "Neural-dynamic-method-based dual-arm CMG scheme with time-varying constraints applied to humanoid robots," *IEEE Trans. Neural Netw. Learn. Syst.*, vol. 26, no. 12, pp. 3251–3262, Dec. 2015.
[28] Y. Zhang, S. S. Ge, and T. H. Lee, "A unified quadratic-programming-based dynamical system approach to joint torque optimization of physically constrained redundant manipulators," *IEEE Trans. Syst., Man, Cybern. B, Cybern.*, vol. 34, no. 5, pp. 2126–2132, Oct. 2004.
[29] D. Guo and Y. Zhang, "A new inequality-based obstacle-avoidance MVN scheme and its application to redundant robot manipulators," *IEEE Trans. Syst., Man, Cybern. C, Appl. Rev.*, vol. 42, no. 6, pp. 1326–1340, Nov. 2012.
[30] Y. Zhang, J. Li, W. Li, and S. Fu, "Complete theory for E47 and 94LVI algorithms solving inequality-and-bound constrained quadratic program efficiently," in *Proc. Chinese Autom. Congr. (CAC)*, Wuhan, China, pp. 183–189, Nov. 2015.
[31] Y. Zhang, X. Lv, Z. Li, Z. Yang, and K. Chen, "Repetitive motion planning of PA10 robot arm subject to joint physical limits and using LVI-based primal-dual neural network," *Mechatronics*, vol. 18, no. 9, pp. 475–485, 2008.
[32] Z. Zhang, L. Zheng, J. Yu, Y. Li, and Z. Yu, "Three recurrent neural networks and three numerical methods for solving a repetitive motion planning scheme of redundant robot manipulators," *IEEE/ASME Trans. Mechatronics*, vol. 22, no. 3, pp. 1423–1434, Jun. 2017.

Zhijun Zhang (Senior Member, IEEE) received the Ph.D. degree from Sun Yat-sen University, Guangzhou, China, in 2012.

He was a Postdoctoral Research Fellow with the Institute for Media Innovation, Nanyang Technological University, Singapore, from 2013 to 2015. From 2015 to 2019, he worked as an Associate Professor, and he has been a Full Professor with the School of Automation Science and Engineering, South China University of Technology, Guangzhou, China, since 2020. He has obtained Guangdong Science Fund for Distinguished Young Scholars, and Youth Talents in Science and Technology Innovation of Guangdong Special Support Plan. He has published more than 80 research papers on the IEEE TRANSACTIONS ON AUTOMATIC CONTROL, the IEEE TRANSACTIONS ON NEURAL NETWORKS AND LEARNING SYSTEMS, the IEEE TRANSACTIONS ON MECHATRONICS, the IEEE TRANSACTIONS ON CYBERNETICS, and top international conferences. His current research interests include neural networks, robotics, machine learning, human machine interaction, and optimal control.

Prof. Zhang is currently an Executive Editor-in-Chief of the *Global Journal of Neuroscience*, an Associate Editor of the *International Journal of Robotics and Control*, a Review Editor of *Frontiers in Robotics and AI*, and reviewers of over 20 international journals. He is currently a member of Committee on Visual Cognition and Computation of Chinese Society of Image Graphics and Hybrid Intelligence Professional Committee of Chinese Association of Automation.

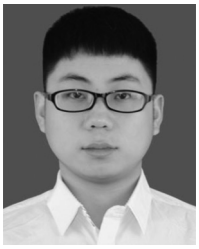

Song Yang received the B.S. degree in automation from the North China Institute of Science and Technology, Langfang, China, in 2018. He is currently pursuing the M.S. degree in control engineering with the School of Automation Science and Engineering, South China University of Technology, Guangzhou, China.

His current research interests include robotics and neural networks.

Siyuan Chen received the B.S. degree in automation from the South China University of Technology, Guangzhou, China, in 2017, where he is currently pursuing the Ph.D. degree in control science and engineering.

His major is motion planning and intelligence system.

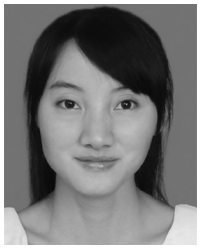

Yamei Luo was born in Shanxi, China, in 1986. She received the M.S. degree from the School of Information Science and Technology, Sun Yat-sen University, Guangzhou, China, in 2015.

In 2012, she joined the Patent Examination Cooperation Center of the Patent Office, SIPO Guangdong, China. She is currently partly working as a Visiting Scholar with the South China University of Technology, Guangzhou. Her current research interests include robotics and intelligent information processing.

Hui Yang received the M.Sc. and Ph.D. degrees from Northeastern University, Shenyang, China, in 1988 and 2004, respectively.

He is a Professor with the School of Electrical and Automation Engineering, East China Jiaotong University, Nanchang, China. His current research interests include intelligent transportation system control, complex system modeling, control and optimization, and process industry integrated automation technology and applications.

Yu Liu (Member, IEEE) received the Ph.D. degree in control engineering from the School of Automation Science and Engineering (SASE), South China University of Technology (SCUT), Guangzhou, China, in 2009.

He was a visiting student with the Department of Mechanical Engineering, Concordia University, Montreal, QC, Canada, from 2008 to 2009, and a Visiting Scholar with the Department of Electrical and Computer Engineering, University of Nebraska–Lincoln, Lincoln, NE, USA, from 2017 to 2018. He is currently a Full Professor with SASE, SCUT. His current research interests include distributed parameter systems, flexible systems, robotics, and machine vision.